



**HAL**  
open science

## Interfaces in 100 epitaxial heterostructures of perovskite oxides

Jean-Luc Maurice, Dominique Imhoff, Jean-Pierre Contour, Christian Colliex

► **To cite this version:**

Jean-Luc Maurice, Dominique Imhoff, Jean-Pierre Contour, Christian Colliex. Interfaces in 100 epitaxial heterostructures of perovskite oxides. *Philosophical Magazine*, 2006, 86 (15), pp.2131-2150. 10.1080/14786430600640460 . hal-00513672

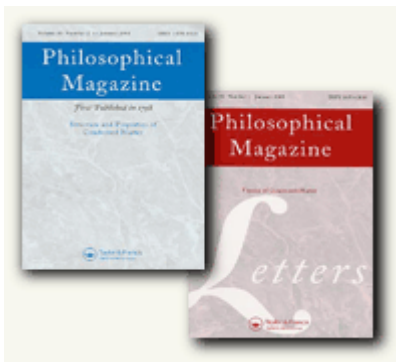
**HAL Id: hal-00513672**

**<https://hal.science/hal-00513672>**

Submitted on 1 Sep 2010

**HAL** is a multi-disciplinary open access archive for the deposit and dissemination of scientific research documents, whether they are published or not. The documents may come from teaching and research institutions in France or abroad, or from public or private research centers.

L'archive ouverte pluridisciplinaire **HAL**, est destinée au dépôt et à la diffusion de documents scientifiques de niveau recherche, publiés ou non, émanant des établissements d'enseignement et de recherche français ou étrangers, des laboratoires publics ou privés.



**Interfaces in {100} epitaxial heterostructures of perovskite oxides**

Journal:	<i>Philosophical Magazine &amp; Philosophical Magazine Letters</i>
Manuscript ID:	TPHM-05-Apr-0112.R1
Journal Selection:	Philosophical Magazine
Date Submitted by the Author:	17-Oct-2005
Complete List of Authors:	Maurice, Jean-Luc; CNRS/Thales, Unité Mixte de Physique (UMR CNRS 137) Imhoff, Dominique; Université Paris Sud, Laboratoire de Physique des Solides (UMR CNRS 8502) Contour, Jean-Pierre; CNRS/Thales, Unité Mixte de Physique (UMR CNRS 137) Colliex, Christian; Université Paris Sud, Laboratoire de Physique des Solides (UMR CNRS 8502)
Keywords:	perovskites, EELS, epitaxy, interfaces, oxide thin films
Keywords (user supplied):	



## Interfaces in {100} epitaxial heterostructures of perovskite oxides

J.-L. MAURICE<sup>11</sup>, D. IMHOFF<sup>2</sup>, J.-P. CONTOUR<sup>1</sup>, C. COLLIEX<sup>2</sup>

<sup>1</sup>Unité Mixte de Physique CNRS<sup>2</sup>/Thales (UMR CNRS 137), Route départementale 128, 91767 Palaiseau cedex, France, and Université Paris-Sud, 91405 Orsay cedex, France.

<sup>2</sup>Laboratoire de Physique des Solides (UMR CNRS 8502), Bât. 510, Université Paris-Sud, 91405 Orsay cedex, France.

### ABSTRACT

The exact perovskite structure has simple cubic symmetry and composition  $ABO_3$ , where A is a relatively large cation and B a smaller one. The choices of A and B cations and the substitutions possible on either site generate a large variety of materials sharing the same base, with relatively small distortions of the size and shape of the cube. As in addition, these oxides often admit oxygen non stoichiometry with or without order to the amount of several per cent, they finally form a vast set of technologically relevant materials: conducting, insulating, ferroelectric, magnetic, superconducting,.... Heteroepitaxy of perovskite oxides allows one to construct atomically sharp interfaces between these materials and therefore to envisage a set of useful heterojunctions. The epitaxy has side effects that may also prove useful: (1) it forces a chemical neighbouring that would not occur naturally, creating a two-dimensional third material, and (2) it imposes a lateral strain. Both of these effects allow one to explore novel, sometimes unforeseen, properties with a strong two-dimensional character. This paper first reviews some of the knowledge that has been accumulated on {100} surfaces and interfaces of perovskites, with an emphasis on properties that could be used in future all-oxide microelectronics. It then exposes the case of the interface between the half-metal  $La_{2/3}Sr_{1/3}MnO_3$  and the insulator  $SrTiO_3$ , which plays a key role in the magnetoresistance of magnetic tunnel junctions. It particularly presents thorough electron energy loss spectroscopy measurements that uncover the atomic scale structural and electronic properties of these objects.

---

<sup>1</sup> Email : jean-luc.maurice@thalesgroup.com

<sup>2</sup> Centre national de la recherche scientifique

## §1. INTRODUCTION

1  
2  
3  
4 Silicon metal oxide semiconductor (MOS) technology has to face in the forthcoming years  
5 what is probably the biggest challenge it has ever met with since Moore predicted its fate in 1965  
6 [1]. Due to the scaling down of circuits, silicon's natural oxide  $\text{SiO}_2$  will no longer fulfil the role of  
7 gate dielectric for transistors: if the trend of Moore's law is maintained, this oxide will shortly reach  
8 a thickness where electron tunnel trespassing becomes significant. This situation creates a unique  
9 opportunity for other candidate materials to replace not only the oxide, but also the whole  
10 technology and the material it is based on. Perovskite epitaxial heterostructures, which exhibit a  
11 wide variety of useful physical properties, are among these.

12  
13  
14  
15  
16  
17  
18  
19  
20  
21 The perovskite family includes insulators with a high dielectric constant (e.g.  $\text{SrTiO}_3$ ) that  
22 can be candidates for use as new gate dielectrics [2, 3]. However, perovskite oxides span a vast  
23 range of physical properties: from insulating to semiconducting, conducting and superconducting, or  
24 in other respects from ferroelectric or piezoelectric to ferromagnetic, etc., depending on their exact  
25 composition. The replacement in standard MOS design of silicon itself by a semiconducting  
26 perovskite is under investigation [4]. This multiplicity is obtained within a same simple crystal  
27 structure never far from simple cubic. To describe the versatility of the family, Smyth [5] has  
28 introduced the concept of 'Perovskite space'. Thanks to the small structural changes from one  
29 compound to the other, they can form atomically sharp interfaces in epitaxy. New devices can thus  
30 be conceived based on their use in both passive and active parts [6-8].

31  
32  
33  
34  
35  
36  
37  
38  
39  
40 Of course, as active regions will always include interfaces, one will want the latter as perfect  
41 as possible. However 'perfect' it may be, an interface at an atomic scale is an assembly of atoms for  
42 which several of the nearest neighbours are 'wrong', so that the physical properties there cannot be  
43 those of either of the two crystals in contact. This interface specificity is particularly important in  
44 heterostructures where a given crystal site can hold atoms of different valencies, as in the case of  
45 diamond and sphalerite semiconductors [9, 10] or indeed perovskites. This gives rise to electrostatic  
46 frustrations – in insulating or semiconducting systems – or more generally to an interface-specific  
47 density of states that may widely differ from that of either of the two crystals in contact, as if the  
48 interface were a third material [11]. In other respects, electrostatic frustration at interfaces is also  
49 well known at grain boundaries of semiconductors [12] or insulators. The interest for this problem  
50  
51  
52  
53  
54  
55  
56  
57  
58  
59  
60

1 in heteroepitaxial perovskite structures is more recent, owing to the more recent development of the  
2 atomic-level control of growth for these materials.  
3  
4

5 The second point that makes heteroepitaxy of perovskites an interesting fundamental study is  
6 the interplay in these materials between the distortions and the electronic structure, through the  
7 Jahn-Teller effect [13, 14]. The epitaxial strain must also be considered as a useful tuning parameter  
8 for the electronic, magnetic or ferroelectric properties [15].  
9  
10  
11  
12

13 The aim of the present paper is to shed some light on these yet little investigated interface-  
14 specific properties. As an example, we present the  $\text{La}_{2/3}\text{Sr}_{1/3}\text{MnO}_3/\text{SrTiO}_3$  (001) interface.  
15  $\text{La}_{2/3}\text{Sr}_{1/3}\text{MnO}_3$  (LSMO) is a ferromagnetic metal where only spin up electrons are present at the  
16 Fermi level ('half metal') [16-18] and  $\text{SrTiO}_3$  (STO) is an insulator. Magnetic tunnel junctions  
17 made of the stacking LSMO/STO/LSMO, where the LSMO layers are ~20-nm thick and the tunnel  
18 STO barrier is ~2-nm thick, have exhibited tunnel magnetoresistance (TMR) ratios of about 2000%  
19 [18]. This magnetoresistance decreases with temperature much faster than the magnetisation of the  
20 two LSMO films. This has been attributed to the interfaces. After an atomic-scale analysis using  
21 electron energy loss spectroscopy (EELS), we propose here to explain how.  
22  
23  
24  
25  
26  
27  
28  
29  
30  
31

32 In section two, we give general information on the perovskite structure, its defects and the  
33 relationships between structure and properties; in section three, we describe how one can grow a  
34 perovskite layer epitaxially on another perovskite and we introduce the importance of the choice of  
35 the terminating atomic layer on which to start the growth. In section four, we present our example of  
36 interface-specific properties in perovskites, which is that of the LSMO/STO (001) interface. We  
37 conclude in section five.  
38  
39  
40  
41  
42  
43  
44  
45  
46  
47

## 48 §2. GENERAL INFORMATION ON PEROVSKITE OXIDES 49

### 50 2.1 Cubic structure 51

52 The perovskite structure has general formula  $\text{ABX}_3$ , where A is a relatively large cation, B a  
53 smaller cation, and X an anion, oxygen in the type compound  $\text{CaTiO}_3$  and in this paper.  
54 Geometrically, the base perovskite unit cell is a cube which can be described in two ways: either  
55 with A ions at the corners and oxygen ions at the centre of the faces forming an octahedral cage  
56 around the B ion in the middle of the cube, or with B ions at the corners and the A ion at the centre  
57  
58  
59  
60

1 of the cube (figure 1). The latter has the advantage of exhibiting the skeleton of corner-sharing  
2 oxygen octahedra. The space group of this base structure is  $Pm\bar{3}m$ . In  $\langle 100 \rangle$  directions, it is a  
3 stacking of  $\{200\}$  planes of alternating compositions AO and  $BO_2$ , which indicates that two types of  
4  
5 stacking of  $\{200\}$  planes of alternating compositions AO and  $BO_2$ , which indicates that two types of  
6  
7  $\{100\}$  surfaces can be found.  
8  
9

## 10 *2.2 Intrinsic distortions*

11 Depending on the size ratio of the ions, the oxygen octahedra are most often distorted,  
12 rotated or tilted over a small range; the results of these distortions can still be described by a pseudo  
13 cubic shape but adopt an orthorhombic (case of  $CaTiO_3$ ) or rhombohedral symmetry (figure 2) [19].  
14  
15 The key parameter that causes these symmetry changes is not directly the ionic charge but the ionic  
16  
17 radius [20].  
18  
19  
20  
21  
22  
23

## 24 *2.3 Distortions and electronic structure*

25 Jahn and Teller [21] have shown that distorting a highly symmetric atomic arrangement may  
26 minimise equilibrium electron energy. The effect that bears their names is particularly active in  
27 perovskites on the oxygen octahedra around B-ions (see e.g. ref. 14). An interesting point is the  
28 coupling by Jahn-Teller effect of the electronic structure with distortions due to epitaxial strain, in  
29 what would be electronic relaxation of strain. The cases where the centre of the oxygen cage is  
30 occupied by a 3d transition metal have especially been studied: for example copper in high-  
31 temperature superconducting cuprates (see e.g. ref. 13), or manganese in colossal-magnetoresistance  
32 manganites [22]. Figure 3 summarises the relationships between the d electron energy levels of a 3d  
33 transition metal at site B, and distortion of the octahedron in the z direction, a symmetry change  
34 typical of the epitaxial strain.  
35  
36  
37  
38  
39  
40  
41  
42  
43  
44  
45  
46  
47  
48  
49

## 50 *2.4 Ionic charge*

51 The sum of the valencies of ions A and B must be six, with that of B greater or equal than  
52 that of A. One has to keep in mind, however, that the picture of six electrons localised on the  
53 oxygen ions and six holes on the cations is an oversimplification; the actual localised charge is  
54 fractional [23]. In keeping with the pseudo cubic arrangement, the choices for A and B ions are  
55 large, as are the possibilities of substitutions on either site and as is the range of oxygen departure  
56 from stoichiometry: this is why perovskite oxides span the vast range of physical properties we have  
57  
58  
59  
60

1 mentioned in introduction. A graph of some of these properties as a function of composition and  
2 point-defect content has been given by Smyth [5].  
3  
4

### 7 §3. HETEROEPITAXY OF PEROVSKITES

#### 10 3.1 Growth technique

11 The deposition techniques for perovskites have undergone a tremendous progress during the  
12 development of high temperature superconductors. Physical as well as chemical deposition methods  
13 were tested. These techniques have been reviewed by Scheel *et al.* [24] for the case of  $\text{YBa}_2\text{Cu}_3\text{O}_{7-x}$ .  
14 A trend towards atomic layer epitaxy, which is necessary for the control of interfaces, has  
15 manifested itself since the beginning of the 1990s [25]. Although classical molecular beam epitaxy  
16 has been utilised [26], atomic layer control can be achieved by an a priori less precise technique  
17 which is pulsed laser deposition (PLD) [25, 27-30]. The reader can find general information on  
18 most of the available techniques in the review papers assembled in the MRS Bulletin of Sept. 1994.  
19  
20  
21  
22  
23  
24  
25  
26  
27

28 We use PLD to prepare LSMO/STO/LSMO junctions such as the one presented in section 4.  
29 Our growth conditions have been described elsewhere [31]. Two points worth mentioning are (1)  
30 that the targets are stoichiometric (so that controlling the surface termination of a growing film is  
31 not directly possible) and (2) that, in the particular case of the LSMO/STO/LSMO stack, the oxygen  
32 partial pressure is maintained during the whole growth at the relatively high value of  $\sim 0.3$  torr ( $\sim 40$   
33 Pa).  
34  
35  
36  
37  
38  
39

#### 42 3.2. Substrate surface

43 In order to obtain eventually an atomically sharp interface, it is necessary to start from a  
44 perfectly flat surface. More precisely, with a view to using the specific properties of a given stacking  
45 sequence, the  $\{100\}$  starting surface must be everywhere of a given type, either AO or  $\text{BO}_2$ . The  
46 unavoidable surface steps associated with miscut must have all the same height of a full unit cell. A  
47 surface step of half a unit cell changes the nature of the surface from AO to  $\text{BO}_2$  (or vice versa) and  
48 is undesirable. Of course in reality, reconstructions occur that move the atomic positions [32, 33].  
49 Here, we only consider the type of sequence that a given surface will provoke, which is given by the  
50 chemical composition of the last  $\{200\}$  plane.  
51  
52  
53  
54  
55  
56  
57  
58  
59

60 The chemical type of the surface can be characterised using different geometries of Rutherford scattering, e.g. low energy ion scattering spectroscopy (LEISS) or coaxial-impact-

1 collision ion-scattering spectroscopy (CAICISS). (These techniques suppose a given atomic order at  
2 the surface, usually that of the bulk.) At a microscopic scale, a given type of surface may be  
3 recognised by measuring the friction force of a tip (friction force microscopy, FFM) [34]. However,  
4 correlating FFM measurements with macroscopic data is not straightforward, so that it is still  
5 necessary to perform one's own calibrations to ascertain whether AO or BO<sub>2</sub> is the toughest. In the  
6 case of the STO (001) surface, Tanaka *et al.*, by monitoring the last single layer deposited in their  
7 layer-by-layer deposition equipment, have found the SrO termination harder [28]. Iwahori *et al.*  
8 have obtained the same result by comparing FFM and CAICISS data [35].

9  
10 The domains of equilibrium (oxygen partial pressure, temperature) of a given termination –  
11 AO or BO<sub>2</sub> – are usually not known. In the case of SrTiO<sub>3</sub> (001), it is generally admitted that an  
12 anneal around 900°C, whether in ultra high vacuum [36] or under oxygen flow [33], produces a  
13 pure TiO<sub>2</sub> surface. Obtaining this surface can also be done by etching in buffered NH<sub>4</sub>F-HF [37].  
14 The problem rests with the obviously less stable SrO-terminated surface. Nakamura *et al.* have  
15 observed by LEISS that the surface of a homoepitaxial STO film, grown by PLD on a substrate  
16 treated with the Kawasaki method [37], was SrO terminated in the conditions they used [38]. Other  
17 authors have used SrO [27, 39] or Sr [28] targets to achieve SrO termination of their STO substrates  
18 or growing films. A drawback of these techniques, especially in the case of SrO target, is that one  
19 does not control whether the (002) atomic plane below the SrO surface plane is TiO<sub>2</sub> as it should, or  
20 if it is another SrO plane as in a Ruddlesden-Popper phase (see next section).

21  
22 In our example of the LSMO/STO/LSMO tunnel junction detailed in section 4, the  
23 termination of the starting LSMO surface was one of the questions to be answered, knowing that we  
24 had no control on the substrate surface termination. The growth of LSMO onto TiO<sub>2</sub>-terminated  
25 STO is well documented. Yoshimoto *et al.* [40] on the one hand, Izumi *et al.* [41] independently,  
26 found by CAICISS that LSMO grown at low pressure on this surface was MnO<sub>2</sub>-terminated. The  
27 more recent work of Kumigashira *et al.* [42], performed by angularly resolved XPS, confirmed this  
28 result and also showed that, on SrO-terminated STO conversely, LSMO was La(Sr)O-terminated.  
29 Quite unfortunately, our case of relatively high pressure growth is poorly documented. Yoshimoto *et*  
30 *al.* mention preliminary experiments where the effect of oxygen pressure would be to stabilise the  
31 La(Sr)O (001) surface [40].

1 The experimental investigation of any novel phenomena related to a given sequence at the  
2 interface poses the difficult problem of preparing surfaces that are unambiguously either AO or  
3 BO<sub>2</sub>: this is probably one of the major challenges in these studies.  
4  
5  
6  
7

### 8 *3.3 Perovskite defects that can be found at epitaxial interfaces*

9 Quite generally, performing the growth of single crystal films without defects is a challenge.  
10 A first source of defects is the mismatch between the crystal parameters of the film and of the  
11 substrate and, as growth is generally performed at high temperature, its differential evolution with  
12 temperature.  
13  
14  
15  
16  
17  
18

19 Perovskite oxides respond very differently to epitaxial strain, depending on their plastic and  
20 elastic properties: for example SrTiO<sub>3</sub> is ductile at room temperature [43], whereas La<sub>2/3</sub>Sr<sub>1/3</sub>MnO<sub>3</sub>  
21 relaxes by fracture when grown at 850°C [44]. In all cases, the solution is to prepare layers thinner  
22 than the critical thickness  $t_c$  (at which a first relaxing defect is introduced, see e.g. ref. 45). The  
23 actual critical thickness in standard growth conditions is usually neatly higher than the one that can  
24 be calculated at equilibrium, which is of the order of 10 nm for a misfit of 1% in the case of STO  
25 [45]. The actual critical thickness in the case of the growth of LSMO on STO (001), where the  
26 parameter misfit is ~0.8%, is ~150 nm [44].  
27  
28  
29  
30  
31  
32  
33  
34

35 It is quite important to note that the strain field of misfit dislocations extends over distances  
36 typically of the order of their period, at least several nm. This field has an important effect in such  
37 materials where bond length and angle are in close relationships with ionic charges, magnetisation  
38 or polarisability. Chu *et al.* have recently shown that distortions by this field in PZT  
39 (Pb(Zr<sub>0.52</sub>Ti<sub>0.48</sub>)O<sub>3</sub>) ferroelectric nanodots had the effect of cancelling the polarisation in the regions  
40 considered [46].  
41  
42  
43  
44  
45  
46  
47

48 In addition to a specific value of the crystal parameter, most perovskites have a specific non-  
49 cubic symmetry so that a given pseudo cubic orientation corresponds to several orientations of the  
50 true rhombohedral or orthorhombic phase, which make as many variants in the film, separated by  
51 twin boundaries. However, twinning disorientations are small and twin boundaries moreover adapt  
52 them over a significant spatial extension [47], so that their effect close to the interface is probably  
53 small compared to the epitaxial strain. The manganite La<sub>2/3</sub>Sr<sub>1/3</sub>MnO<sub>3</sub> that is the object of section 4  
54 is rhombohedral (figure 2) – and twinned in epitaxial films (see ref. [44] for details).  
55  
56  
57  
58  
59  
60

1  
2  
3  
4  
5  
6  
7  
8  
9  
10  
11  
12  
13  
14  
15  
16  
17  
18  
19  
20  
21  
22  
23  
24  
25  
26  
27  
28  
29  
30  
31  
32  
33  
34  
35  
36  
37  
38  
39  
40  
41  
42  
43  
44  
45  
46  
47  
48  
49  
50  
51  
52  
53  
54  
55  
56  
57  
58  
59  
60

Another defect which is specific to perovskites originates in the deposition of ‘wrong’ ions in the first layer (A instead of B or inversely). It leads to a fault in the perovskite stacking sequence at the interface. It can be either an  $A_fO$  layer on an AO-terminated surface, or a  $B_fO_2$  layer on a  $BO_2$ -terminated surface (where the index  $f$  indicates that the ion of type A or B belongs to the growing film). We are not aware of occurrences of the latter, while the former exists as stacking fault in bulk perovskites. The additional AO plane is then laterally shifted by  $\frac{1}{2}\langle 110 \rangle$  (where the indices refer to the perovskite cube). Structurally, it is equivalent to the replacement in the perovskite  $\langle 100 \rangle$  sequence of an AO atomic plane by half a rock-salt unit cell of the compound AO; the new sequence actually forms stable phases when repeated, as described by Ruddlesden and Popper [48, 49]. As mentioned in the previous section, the occurrence of such a fault would not be surprising when depositing the rock-salt compound AO on an  $ABO_3$  perovskite substrate.

#### §4. THE LSMO/STO/LSMO (001) INTERFACES

##### 4.1 Generalities

Tunnel magnetoresistance (TMR) of a magnetic tunnel junction depends on the polarisation of tunnelling electrons [50]. These particles essentially originate from the very last layer of conductive material, at each interface of the two sides of the barrier. It is therefore of prime importance to know how the interfaces modify the bulk properties.

In the case of magnetic perovskites such as manganites, magnetism and transport are related to the mixed-valency of B ions ( $Mn^{3+/4+}$  in LSMO), which in turn depends on the valencies of the surrounding A ions ( $2/3 La^{3+}$  and  $1/3 Sr^{2+}$  in LSMO). Ion B may be directly at the interface (type II in our previous work [51]) or ‘protected’ by an AO layer of its own material (type I in ref. 51). If the manganite is deposited first, type I corresponds to the configuration of figure 4a, and type II to that of figure 4b. In a sketchy approach, type I, where B (Mn) ions have bulk environment, will be less detrimental to the magnetic properties of the last layer than type II, where the environment of B ions at the interface is ‘wrong’ for half of it [52]. We shall see below that the two types actually correspond to opposite charge transfers, which will both modify the materials properties.

#### 4.1.1 Electrostatic equilibrium

In order to introduce the electrostatic side of the problem, let us briefly consider a case that has been the object of several works: that of the (001) interface between the insulating perovskites  $\text{La}^{3+}\text{Al}^{3+}\text{O}_3$  (LAO) and  $\text{Sr}^{2+}\text{Ti}^{4+}\text{O}_3$  [27, 39]. When looking at the stacking in the [001] direction, LAO is an alternating pile-up of  $\text{La}^{3+}\text{O}^{2-}$  and  $\text{Al}^{3+}\text{O}^{2-}_2$  planes, which carry respectively an electric charge of  $+|e|$  and  $-|e|$  per unit cell area, where  $|e|$  is the positive elementary charge. Whilst on the other hand, STO in this direction is a stacking of  $\text{Sr}^{2+}\text{O}^{2-}$  and  $\text{Ti}^{4+}\text{O}^{2-}_2$  planes that are both neutral. Because the (002) planes are not electrostatically equivalent in LAO and STO, the (001) interface must carry a ‘frustration’ charge depending on the exact stacking sequence. To keep the configuration of figure 4, let LAO be the substrate; the two following cases can occur: (type I) the starting surface is LaO-terminated as in figure 4a, or (type II) the starting surface is  $\text{AlO}_2$ -terminated as in figure 4b. In a strictly ionic view with fixed valencies, the former corresponds to doping the structure with half an electron per unit surface cell, and the latter with half a hole. In order to experimentally study these two interfaces, Ohtomo and Hwang have prepared an STO (001) substrate with either  $\text{TiO}_2$ -termination or SrO-termination, for respectively the interfaces of type I and II, and deposited LAO on it. If they did not obtain a doping effect with type II, they indeed obtained a tremendous (actually greater than  $1/2$  per unit cell) n-doping with type I interface (sequence:  $\text{AlO}_2/\text{LaO}/\text{TiO}_2/\text{SrO}$ ), with quite high mobilities at low temperature [39].

Although one of the films is conducting in our LSMO/STO interfaces, it is quite useful to submit them to the same analysis, just by replacing LAO by LSMO. Nominally in LSMO, in the absence of oxygen vacancies, the  $\text{Mn}^{3.3+}\text{O}^{2-}_2$  planes have an average electrostatic charge of  $-2/3|e|$  per unit cell area and the  $\text{La}^{3+}_{2/3}\text{Sr}^{2+}_{1/3}\text{O}^{2-}$  ones have a charge of  $+2/3|e|$  per unit cell. In such a case, the charge at the interface would be  $+|e|/3$  per unit cell in the case of type I ( $\text{MnO}_2/\text{La}_{2/3}\text{Sr}_{1/3}\text{O}/\text{TiO}_2/\text{SrO}$ ), or  $-|e|/3$  in the case of type II ( $\text{La}_{2/3}\text{Sr}_{1/3}\text{O}/\text{MnO}_2/\text{SrO}/\text{TiO}_2$ ), and in turn this would inject  $1/3$  electron per unit cell in the former case, and  $1/3$  hole in the latter. However as both Ti and Mn are mixed-valency ions, the actual charge at the interface would depend on whether these carriers be mobile or trapped by the cations, thus moving their valencies. Now introducing the fact that LSMO precisely carries charges by changing the valency of Mn ions, we can give more precision to the picture. In the interface of type I, the valency of Ti ions at the interface would be shifted towards  $3+$ , or the released electrons would travel into LSMO and shift

1  
2 the valency of Mn ions over a screening length, on average also towards 3+. In the interface of type  
3  
4 II on the contrary, the Mn ions at the interface would see their valency shifted on average towards  
5  
6 4+.

#### 7 8 *4.1.2 Tunnel magnetoresistance*

9  
10 Tunnel magnetoresistance across a manganite/STO/manganite trilayer was first  
11 demonstrated by Sun *et al.* [16]. Our work originated in electron transport experiments carried out  
12 by Viret *et al.* [17] on devices based on two electrodes of LSMO. The tunnel barrier was a two to  
13 three-nm thick insulating layer that could be made of either  $\text{PrBa}_2(\text{CuGa})_3\text{O}_7$ ,  $\text{CeO}_2$  or  $\text{SrTiO}_3$ .  
14 These structures were grown epitaxially by PLD. The highest magnetoresistance was obtained with  
15 STO as barrier material, but a sharp decrease was observed above 150 K (while the Curie  
16 temperature of the LSMO layers was above 350 K), which was attributed to oxygen vacancies in the  
17 vicinity of the interfaces [17]. Some progress has been made since then, but the electron polarisation  
18 still decreases faster at the interfaces than in the bulk with temperature [18, 53].  
19  
20  
21  
22  
23  
24  
25  
26  
27  
28

#### 29 30 *4.2 Transmission electron microscopy*

31  
32 In order to understand the origin of this decrease well below Curie point, we have carried out  
33 a set of structural measurements by high resolution transmission electron microscopy (HRTEM) on  
34 the one hand, and of chemical and electronic measurements by electron energy loss spectroscopy  
35 (EELS) with the subnanometre probe of a scanning transmission electron microscope (STEM) on  
36 the other hand. We have first analysed the structure and composition of the very junction measured  
37 by Viret *et al.* [17]. Then, in order to study the residual Mn and La EELS signals collected after the  
38 apex of the interfaces into the barrier down to zero intensity, we have prepared the same system in  
39 identical conditions, where the STO barrier was 5.5 nm thick (figure 5).  
40  
41  
42  
43  
44  
45  
46  
47

48 Most of the results of our microscopic investigations have already been published in papers  
49 where the reader can find all the technical details concerning our experimental conditions [47, 51,  
50 52, 54]. In the present paper, these results are revisited, and with the support of quite recent  
51 publications [55], some routes can be eliminated as possible explanations for the observed  
52 behaviour.  
53  
54  
55  
56  
57  
58  
59  
60

### 4.3 Electron energy loss spectroscopy

We focus here on EELS core edges. In such signals, the energy lost by incident electrons is transferred to core-level electrons that jump to energy levels in the conduction band above the Fermi level. As core levels are very narrow in energy, EELS core edges give in a first order approximation an image of the density of states immediately above the Fermi level, i.e. the density of *empty* states in the conduction band. In this study, several different edges were recorded and will be discussed in detail, and we will see how this simple approach has to be accepted or modified as a function of the electron levels involved in the transition.

In order to correlate unambiguously the recorded EELS spectra with their exact location of origin in the sample, the spectrum-imaging mode [56] has been used in a VG STEM microscope. This instrument is equipped with a cold field emission source, delivering a minimum probe size of 0.5 nm, with a digitally controlled scanning unit, which can raster the incident probe over the investigated area (1D or 2D patterns and a position displacement step down to 0.2 nm) and a parallel EELS spectrometer including a new generation of CCD detector. For each probe position, EELS spectra are acquired over an energy-loss spectral domain incorporating all edges of interest, within typical recording times from tens to hundreds milliseconds for each core-loss spectrum with sufficiently high signal-to-noise ratio to be sensitive to weak changes of fine structures. These huge data sets are analysed and processed *a posteriori*, using the software that has been developed in our group for elemental mapping, energy loss deconvolution and multivariate statistical analysis. Selected results extracted from these measurements are presented and discussed below. Figure 6a shows a sequence of spectra corresponding to the transition at the interface between the bottom LSMO layer and the insulating layer. Details of the evolution of the fine structures on the three most important signals O-K, Mn-L<sub>2,3</sub> and Ti-L<sub>2,3</sub> are extracted for more specific analysis (figures 6b, c and d).

As a general observation, there is no significant difference in any monitored EELS spectral feature between the top and bottom interfaces. This will be considered in section 4.3.3.

A second result is that, when going from the bulk of the LSMO film to the interface, the chemical shift of the Mn-L<sub>2,3</sub> edge is small and towards *lower* energy losses (see figure 9). When compared to the reference work of Abbate *et al.* [57], this result means that the MnO<sub>2</sub> planes are reduced, or electron-doped, in the vicinity of the interface. In our previous publications [51, 52, 54],

1 we had explored several explanation of this electron doping. We had considered segregation  
2 between the La and Sr cations of LSMO (so that there be a higher La/Sr ratio in the vicinity of the  
3 interface) and finally excluded it in regard to our recorded elemental profiles [54]. We had also  
4 discussed the presence oxygen vacancies in the vicinity of the interface, as proposed by Viret *et al.*  
5 [17]. We were not able to precisely define the main origin of electron doping.  
6  
7  
8  
9  
10  
11

12 We can now propose a new interpretation scheme following which the electron doping of  
13 LSMO at the interface with STO is essentially due to the fact that the stacking sequence is  
14  $\text{La}_{0.7}\text{Sr}_{0.3}\text{O}/\text{TiO}_2$  (type I), for which electrostatic equilibrium imposes the presence of extra  
15 electrons at the interface (see section 4.1.1). This result is opposite to the hole-doped (type II)  
16 configuration assumed by Yamada *et al.* [58] in a recent study of the same interface. This  
17 discrepancy might be related to different growth conditions. Let us now examine all the above  
18 mentioned possibilities versus our detailed EELS measurements.  
19  
20  
21  
22  
23  
24  
25

#### 26 4.3.1 La/Sr ratio at the STO/LSMO interface

27 Figure 7a shows an EELS map exhibiting the ratio of the La-4d and Sr-4p signals over a  
28 square area incorporating the two LSMO films on both sides of the STO tunnel junction. It does not  
29 show any significant variations over the analysed area in the bulk of the LSMO films. This is quite  
30 obvious when we plot profiles across this region, integrated over a few profiles perpendicular to the  
31 junction (see figure 7b). Both La/Sr and Mn curves have the half of their maximum value at the  
32 same probe positions and the distance between these half maximum value positions corresponds to  
33 5.5 nm, within an accuracy better than 0.5 nm, i.e. the width of the insulating STO layer deduced  
34 from HRTEM (figure 5) or annular dark field images. It clearly indicates that there is no increase of  
35 the La/Sr ratio in the vicinity of the interface.  
36  
37  
38  
39  
40  
41  
42  
43  
44  
45  
46

#### 47 4.3.2 Oxygen concentration at the STO/LSMO interface

48 The departures of oxygen concentration from stoichiometry are much more difficult to  
49 assess. However, they can be searched for in the evolution of different signals when the beam is  
50 scanned across the interfaces. It can be directly on the O-K edge or indirectly in the associated  
51 transition metal L lines. Let us consider first the family of four spectra exhibiting the detailed profile  
52 of the oxygen K-edge, recorded on both reference materials LSMO and STO and at the apex of the  
53 two interfaces (bottom and top along the growth direction of the multilayer) (figure 8a). These last  
54 two are in excellent agreement, and they can be simulated as a linear combination of the two  
55  
56  
57  
58  
59  
60

1 reference ones, with a weighting factor depending on the exact probe position. Non negative least  
2 square fit and multivariate statistical analysis reveal no new interface signal different from the  
3 mixing between LSMO and STO.  
4  
5  
6

7  
8 Muller *et al.* [55] have studied the evolution of the oxygen K edge for various oxygen  
9 deficient strontium titanate foils ( $\text{SrTiO}_{3-\delta}$  with  $\delta$  varying from 0 to 0.25). The spectra that they have  
10 recorded are shown in figure 8b for comparison with our spectra. The presence of oxygen vacancies  
11 in the STO layer when approaching the interfaces should appear through a broadening of the first  
12 line towards higher energy loss values and a vanishing of the second peak around 536 eV, which is  
13 contrary to the behaviour we observe. This effect constitutes a first hint of the absence of oxygen  
14 vacancies at the interfaces. However, one must recognize that it is difficult to extract definitive  
15 conclusions when considering only the O-K edge, because it is the dominant element present  
16 everywhere and weak variations in signal shape could be obscured by the general change of the O-K  
17 ELNES signal when evolving from the STO environment to the LSMO one.  
18  
19  
20  
21  
22  
23  
24  
25  
26  
27

28  
29 An alternative solution, still in the STO layer, is to look for changes of the Ti  $L_{23}$  lines when  
30 approaching the interface, while this signal drops to zero (no Ti present in the LSMO layers). Two  
31 spectra recorded at the top and bottom interfaces are superposed in figure 8c, after proper rescaling,  
32 on a spectrum corresponding to the centre of the STO tunnel barrier. No significant change can  
33 again be detected, while Muller *et al.* [55] have shown that the presence of oxygen vacancies should  
34 give a significant one: the four Ti  $L_{23}$  lines, clearly resolved in vacancy-free STO and in our  
35 measurements, should broaden, mix and shift as the oxygen vacancy level ( $\delta$ ) increases (figure 8d).  
36  
37  
38  
39  
40  
41  
42

43  
44 The typical splitting of Ti-2p in four lines correspond to the superposition (figure 6d) of  
45 intra-atomic effects giving rise to two major lines corresponding to the excitation of the Ti  $2p_{1/2}$  ( $L_2$ )  
46 and  $2p_{3/2}$  ( $L_3$ ), and of the crystal field effect inducing the extra splitting into  $t_{2g}$  and  $e_g$  states (see  
47 figure 3). The presence of oxygen vacancies should indeed change these shapes for several reasons:  
48 shift of the average valency of Ti ions from 4+ to 3+, introduction of extra Jahn-Teller contributions  
49 to the splitting of the lines either directly or through the induced crystal structure distortions (figure  
50 3). More generally, electron doping of STO would bring a change characteristic of the presence of  
51  $\text{Ti}^{3+}$  in the Ti-2p edge [59]  
52  
53  
54  
55  
56  
57  
58

59  
60 None of these effects occur here. On the contrary, the stability of the detailed shape of the  
STO Ti  $L_{2,3}$  signal, from the centre of barrier to the interfaces, is quite remarkable on the spectra

1 shown in figure 8c, where the energy resolution has been improved down to 0.4 eV using the  
2 deconvolution methods developed by Gloter *et al.*[60]. The clear conclusion at this stage is thus that  
3 the concentration of oxygen vacancies in the whole STO layer, up to both interfaces, is close to  
4 zero. This statement is consistent with the high-pressure growth conditions (section 3.1).  
5  
6  
7  
8  
9

10 Applying the same methodology to the manganese  $L_{2,3}$  signal for tracking the possible  
11 presence of oxygen vacancies on the LSMO side of the interfaces is less favourable for several  
12 reasons associated with the fact that the 3d band is not empty in LSMO. Simple arguments on the  
13 nature and distribution of empty d states can no longer be used, because as shown by Kurata and  
14 Colliex [61] the white line profiles such as the Mn  $L_3$  one are strongly influenced by intra-atomic  
15 correlation effects due to the coupling between the p hole and the d orbitals. We shall see below,  
16 however, that oxygen vacancies are not necessary to shift Mn valency and drop the electron  
17 polarisation at the interfaces.  
18  
19  
20  
21  
22  
23  
24  
25

#### 26 4.3.3 The Mn-2p signal at the interface

27 Let us now focus on the evolution of the Mn- $2p_{3/2}$  ( $L_3$ ) line at the interface. Figure 9  
28 exacerbates the separation into two peaks as the displayed spectra correspond to a second derivative  
29 mode. Practically in the bulk of the film, the major peak lies at 642 eV and the secondary peak,  
30 which is nearly invisible in the bulk LSMO phase in normal mode, points out about 1.8 eV below.  
31 When approaching the interfaces with STO, the peak splitting decreases by 0.2 eV and the  
32 secondary peak is sharper and its intensity increases. This is valid for both the top and bottom  
33 interfaces as they appear here as in other measurements quite symmetrical and equivalent.  
34  
35  
36  
37  
38  
39  
40  
41  
42

43 In our previous paper dedicated to EELS [54], we have thoroughly discussed this evolution,  
44 notably with reference to the work of Abbate *et al.* [57]. We can now complete our comparisons.  
45 Abbate *et al.* have recorded reference spectra of Mn-2p in the series  $La_{1-x}Sr_xMnO_3$  using X-ray  
46 absorption, with  $x$  varying from 0 to 0.9, i.e. Mn valency varying from 3+ to almost 4+ [57]. They  
47 paid a special attention to the two extreme compositions still compatible with the perovskite  
48 structure, namely  $La_{0.1}Sr_{0.9}MnO_3$  and  $LaMnO_3$ , for which they fitted the experimental spectra with  
49 multiplet calculations. Two peaks are present in these calculated and experimental Mn- $L_3$  lines, very  
50 much like in the present EELS spectra. In the series of spectra they have recorded, as the valency of  
51 Mn ion goes from 3+ to 4+, the Mn- $L_3$  signal undergoes essentially two monotonic changes: (1) the  
52 maximum of the Mn  $L_3$  peak shifts by 1 eV towards higher energies, and (2) the splitting between  
53  
54  
55  
56  
57  
58  
59  
60

1 the two peaks also increases from 1.5 to 2.4 eV [57]. As in our case the maximum shifts towards  
2 lower energies and the peak splitting decreases, we conclude that the  $\text{Mn}^{3+}/\text{Mn}^{4+}$  ratio increases at  
3 the interface, or else, that the last  $\text{MnO}_2$  plane in LSMO is electron donated. The apparent increase  
4 of the pre-peak intensity in figure 9 is not associated with an increase of the splitting between the  
5 two peaks. In our previous work [54], we had proposed that it could be of essentially structural  
6 origin, due to the effect of the epitaxial strain on the distortion of  $\text{MnO}_6$  octahedra. Actually two  
7 effects, the increased  $\text{Mn}^{3+}/\text{Mn}^{4+}$  ratio and the topology, should reinforce the Jahn-Teller splitting at  
8 the interface. In absence of proof, we maintain our earlier proposal that the origin of the  
9 enhancement of the low energy peak could be Jahn-Teller effect.

10 Regarding now the symmetry of the top and bottom interfaces, it implies that the first LSMO  
11 film ends up by an AO plane (viz.  $\text{La}_{0.7}\text{Sr}_{0.3}\text{O}$ ), and that the thin STO layer ends up on the contrary  
12 with a  $\text{BO}_2$  plane (viz.  $\text{TiO}_2$ ). We have attributed this reversal to the fact that in the growth  
13 conditions used, these surfaces would be thermodynamically stable in respectively LSMO and STO.  
14 This is actually confirmed by the preliminary experiment of Yoshimoto *et al.* [40], in the case of  
15 LSMO, while  $\text{TiO}_2$  is very likely the most stable in STO (see section 3.2).

#### 33 4.4. Discussion

34 To summarise, we have shown with a careful analysis of EELS experiments that the Mn ions  
35 at the LSMO/STO interface present a modified d-band compared to the bulk of LSMO films. The  
36 EELS Mn- $L_3$  line exhibits a negative energy shift and a decreased splitting between its two main  
37 features, which we have attributed to an increased ratio of  $\text{Mn}^{3+}$  or electron doping. Conversely, we  
38 have associated the greater sharpness of the minor peak with the interfacial distortion. The only  
39 sequence compatible with the increased ratio of  $\text{Mn}^{3+}$  is  $\text{MnO}_2/\text{La}_{0.7}\text{Sr}_{0.3}\text{O}/\text{TiO}_2/\text{SrO}$  (type I). We  
40 attribute the shift towards 3+ to a transfer of electrons from the  $\text{TiO}_2$  plane of STO, in contact with  
41 the  $\text{La}_{0.7}\text{Sr}_{0.3}\text{O}$  plane, towards the  $\text{MnO}_2$  plane of LSMO.

42 The LSMO/STO interface has been compared, regarding its ferromagnetism, to interfaces of  
43 LSMO with other oxides. Yamada *et al.*[58] have used the sensitivity to surface magnetism of  
44 second harmonic generation to probe the interface magnetism of LSMO/STO, LSMO/LAO, and  
45 LSMO/two unit-cell LMO( $\text{LaMnO}_3$ )/STO. They have found that the interface magnetisation was  
46 the lowest for LSMO/STO, with the fastest decrease with temperature. They interpreted their results  
47 on the assumption that the LSMO/STO interface was a hole donator in their case. It is important to  
48  
49  
50  
51  
52  
53  
54  
55  
56  
57  
58  
59  
60

1  
2  
3  
4  
5  
6  
7  
8  
9  
10  
11  
12  
13  
14  
15  
16  
17  
note that both possible types of interface – type I (electron donating like here), or type II (hole  
donating, like in the work of Yamada *et al.* [58]) – tend to create layers of properties equivalent to  
those of  $\text{La}_{1-x}\text{Sr}_x\text{MnO}_3$  with  $x \neq 0.33$ . As  $x$  departs from 0.33 towards smaller values like here  
(electron doping), or towards higher values (hole doping),  $\text{La}_{1-x}\text{Sr}_x\text{MnO}_3$  has no longer the  
ferromagnetic properties of LSMO (see e.g. figure 49 in [22]). With such a view, both our approach  
and that of Yamada *et al.* [58] explain the decrease of magnetism at the interface. Such a conclusion  
is however no surprise when considering that the double exchange between Mn ions, at the basis of  
magnetism in LSMO, must be frustrated at an interface, be it of type I or II.

18  
19  
20  
21  
22  
23  
24  
25  
26  
27  
28  
29  
30  
31  
32  
33  
34  
35  
36  
37  
38  
39  
40  
41  
42  
43  
44  
45  
46  
47  
48  
49  
50  
51  
52  
53  
54  
55  
56  
57  
58  
59  
60  
On the other hand, Garcia *et al.* [53] have measured the tunnel magnetoresistance of  
junctions made of LSMO/STO/LSMO, LSMO/LAO/LSMO, and LSMO/TiO<sub>2</sub>/LSMO. In that case  
again, although the low-temperature TMR was higher for the STO barrier, its decrease as the  
temperature increased was faster than for the LAO one. These junctions were made by one of us in  
the conditions used for the samples presented here, so that one can assume the same  $\text{La}_{0.7}\text{Sr}_{0.3}\text{O}$   
termination of LSMO in all junctions. Thus the LSMO/LAO interface would correspond to the  
sequence  $\text{MnO}_2/\text{La}_{0.7}\text{Sr}_{0.3}\text{O} // \text{AlO}_2/\text{LaO}$ , for which electrostatic equilibrium would impose extra  
holes. The latter could therefore be less detrimental to the magnetism of LSMO than the electrons  
donated by LSMO/STO.

Finally, *Ab-initio* calculations of the different types of interface configurations would be very  
helpful to fully understand the physics of these systems.

## §5. CONCLUSIONS AND PERSPECTIVES

The goal of the present paper was to exhibit some of the latest advances in the preparation  
and characterisation of perovskite epitaxial heterostructures. These materials present a very large set  
of potentialities. Perovskite heterojunctions have been realised to obtain magnetoresistive devices  
[16-18], MOS structures [4], or 2-dimensional conduction at the interface between two insulators  
[39]. The effects of heteroepitaxial interfaces on ferroelectricity or bi-ferroicity of perovskites are  
starting to be explored [15]. Although the heteroepitaxy of perovskites is now a mature subject as it  
started in the late 1980s with the high temperature superconductors, the atomic-level control of it is  
only beginning. It appears as a wide field of research, with potential applications in very different  
areas of the microelectronics world, from ferroelectric memories to the devices that will replace

1 CMOS technology. The greatest challenge at this beginning is for thin-film growers. A {100}  
2 perovskite surface has two variants: this makes it so interesting, but controlling surface termination  
3 means controlling the deposition of half a unit cell. This is, to our mind, where the biggest effort is  
4 needed. Then come the means of characterising the heterostructures obtained. We hope to have  
5 shown here, that in this regard EELS, performed with a subnanometre probe, is a unique tool that  
6 allow one to know altogether the nature, the valency, and somehow the site symmetry of the ions  
7 present at the interface.  
8  
9  
10  
11  
12  
13  
14  
15  
16

#### 17 ACKNOWLEDGEMENTS

18 The authors wish to thank M. Bibes (Institut d'Electronique Fondamentale, Orsay, France),  
19 A. Barthélémy and A. Fert (UMP CNRS/Thales), for fruitful discussions, A. Gloter (LPS Orsay) for  
20 critical reading of the manuscript, and É. Jacquet (UMP CNRS/Thales) for the PLD growth.  
21  
22  
23  
24  
25

#### 26 REFERENCES

- 27  
28 [1] G. E. Moore, *Electronics* **38** 114 (1965).  
29  
30 [2] C. Först, C. R. Ashman, K. Schwarz, P. E. Blöchl, *Nature* **427** 53 (2003).  
31  
32 [3] J. Robertson, *Euro. Phys. J. Appl. Phys.* **28** 265 (2004).  
33  
34 [4] K. Ueno, I. H. Inoue, T. Yamada, H. Akoh, Y. Tokura, H. Takagi, *Appl. Phys. Lett.* **84** 3726  
35 (2004).  
36  
37 [5] D. M. Smyth, *Cryst. Latt. Def. and Amorph. Mat.* **18** 355 (1989).  
38  
39 [6] J. Zhang, H. Tanaka, T. Kawai, *Appl. Phys. Lett.* **80** 4378 (2002).  
40  
41 [7] A. G. Schrott, J. A. Misewich, R. Ramesh, V. Nagarajan, *Mat. Res. Soc. Symp. Proc.* **747**  
42 V3,8,1 (2003).  
43  
44 [8] K. Shibuya, T. Ohnishi, M. Kawasaki, H. Koinuma, M. Lippmaa, *Mat. Res. Soc. Symp. Proc.*  
45 **747** V3,2,1 (2003).  
46  
47 [9] G. A. Baraff, J. A. Appelbaum, D. R. Hamann, *Phys. Rev. Lett.* **38** 237 (1977).  
48  
49 [10] T. Wang, N. Moll, K. Cho, J. D. Joannopoulos, *Phys. Rev. Lett.* **82** 3304 (1999).  
50  
51 [11] S. Okamoto, A. J. Millis, *Nature* **428** 630 (2004).  
52  
53 [12] J.-L. Maurice, *Philos. Mag. A* **68** 951 (1993).  
54  
55 [13] B. Raveau, C. Michel, M. Hervieu, D. Groult, *Springer series in materials science* **15** (1991).  
56  
57 [14] A. J. Millis, *Nature* **392** 147 (1998).  
58  
59  
60

- 1  
2 [15] C. Thiele, K. Dörr, L. Schultz, E. Beyreuther, W.-M. Lin, submitted.  
3  
4 [16] J. Z. Sun, W. J. Gallagher, P. R. Duncombe, L. Krusin-Elbaum, R. A. Altman, A. Gupta, Y.  
5  
6 Lu, G. Q. Gong, G. Xiao, Appl. Phys. Lett. **69** 3266 (1996).  
7  
8 [17] M. Viret, M. Drouet, J. Nassar, J.-P. Contour, C. Fermon, A. Fert, Europhys. Lett. **39** 545  
9  
10 (1997).  
11  
12 [18] M. Bowen, M. Bibes, A. Barthélémy, J.-P. Contour, A. Anane, Y. Lemaître, A. Fert, Appl.  
13  
14 Phys. Lett. **82** 233 (2003).  
15  
16 [19] R. S. Roth, J. Res. Natl. Bur. Std. **58** 75 (1957).  
17  
18 [20] V. M. Goldschmidt, Skrifter Norske Videnskaps-Akad. Mat. Naturv. Kl. **2** 8 (1926).  
19  
20 [21] H. A. Jahn, E. Teller, Proc. R. Soc. A **161** 220 (1937).  
21  
22 [22] J. M. D. Coey, M. Viret, S. von Molnár, Adv. Phys. **48** 167 (1999).  
23  
24 [23] M. Coey, Nature **430** 155 (2004).  
25  
26 [24] H. J. Scheel, M. Berkovski, B. Chabot, J. Cryst. Growth **115** 19 (1991).  
27  
28 [25] M. Y. Chern, A. Gupta, B. W. Hussey, Appl. Phys. Lett. **60** 3045 (1992).  
29  
30 [26] F. Arrouy, J.-P. Locquet, E. J. Williams, E. Mächler, R. Berger, C. Gerber, C. Monroux, J.-C.  
31  
32 Grenier, A. Wattiaux, Phys. Rev. B **54** 7512 (1996).  
33  
34 [27] D.-W. Kim, D.-H. Kim, B.-S. Kang, T. W. Noh, D. R. Lee, K.-B. Lee, Appl. Phys. Lett. **74**  
35  
36 2176 (1999).  
37  
38 [28] H. Tanaka, H. Tabata, T. Kawai, Thin Solid Films **342** 4 (1999).  
39  
40 [29] G. Rijnders, G. Koster, V. Leca, D. H. A. Blank, H. Rogalla, Appl. Surf. Sci. **168** 223 (2000).  
41  
42 [30] A. Ohtomo, D. A. Muller, J. L. Grazul, H. Y. Hwang, Nature **419** 378 (2002).  
43  
44 [31] J. P. Contour, C. Sant, D. Ravelosona, B. Fischer, L. Patlagan, Jap. J. Appl. Phys **32** 1134  
45  
46 (1993).  
47  
48 [32] G. Renaud, Surf. Sci. Reports **32** 1 (1998).  
49  
50 [33] N. Erdman, K. R. Poepelmeier, M. Asta, O. Warschkow, D. E. Ellis, L. D. Marks, Nature **419**  
51  
52 55 (2002).  
53  
54 [34] J. Fompeyrine, R. Berger, H. P. Lang, J. Perret, E. Mächler, Ch. Gerber, J.-P. Locquet, Appl.  
55  
56 Phys. Lett. **72** 1697 (1998).  
57  
58 [35] K. Iwahori, S. Watanabe, M. Kawai, K. Mizuno, K. Sasaki, M. Yoshimoto, Appl. Phys. Lett.  
59  
60 **88** 7099 (2000).

- 1 [36] W. Maus-Friedrichs, M. Friedrichs, A. Gunhold, S. Krischok, V. Kempter, G. Bihlmayer, Surf.  
2 Sci. **515** 499 (2002).  
3  
4  
5 [37] M. Kawasaki, K. Takahashi, T. Maeda, R. Tsuchiya, M. Shinohara, O. Ishiyama, T. Yonesawa,  
6 M. Yoshimoto, H., Koinuma, Science **266** 1540 (1994).  
7  
8  
9 [38] T. Nakamura, H. Inada, M. Iiyama, Appl. Surf. Sci. **130-132** 576 (1998).  
10  
11 [39] A. Ohtomo, H. Y. Hwang, Nature **427** 423 (2004).  
12  
13 [40] M. Yoshimoto, H. Maruta, T. Ohnishi, K. Sasaki, H. Koinuma, Appl. Phys. Lett. **73** 187  
14 (1998).  
15  
16 [41] M. Izumi, Y. Konishi, T. Nishihara, S. Hayashi, M. Shinohara, M. Kawasaki, Y. Tokura, Appl.  
17 Phys. Lett. **73** 2497 (1998).  
18  
19 [42] H. Kumigashira, K. Horiba, H. Ohguchi, K. Ono, M. Oshima, N. Nakagawa, M. Lippmaa, M.  
20 Kawasaki, H. Koinuma, Appl. Phys. Lett. **82** 3430 (2003).  
21  
22 [43] P. Gumbsch, S. Taeri-Baghdarani, D. Brunner, W. Sigle, M. Rühle, Phys. Rev. Lett. **87**  
23 085505 (2001).  
24  
25 [44] J.-L. Maurice, F. Pailloux, A. Barthélémy, O. Durand, D. Imhoff, R. Lyonnet, A. Rocher, J.-P.  
26 Contour, Philos. Mag. **83** 3201 (2003).  
27  
28 [45] J.-P. Contour, A. Abert, A. Défossez, SPIE **2697** 339 (1996).  
29  
30 [46] M.-W. Chu, I. Szafraniak, R. Scholz, C. Harnagea, D. Hesse, M. Alexe, U. Gösele, Nature  
31 Mater. **3** 87 (2004).  
32  
33 [47] R. Lyonnet, J.-L. Maurice, M. J. Hÿtch, D. Michel, J.-P. Contour, Appl. Surf. Sci. **162-163** 245  
34 (2000).  
35  
36 [48] S.N. Ruddlesden, P. Popper, Acta Cryst. **10** 538 (1957).  
37  
38 [49] S. N. Ruddlesden, P. Popper, Acta Cryst. **11** 54 (1958).  
39  
40 [50] M. Julière, Phys. Lett. **A 54** 225 (1975).  
41  
42 [51] J.-L. Maurice, F. Pailloux, D. Imhoff, N. Bonnet, L. Samet, A. Barthélémy, J.-P. Contour, C.  
43 Colliex, A. Fert, Euro. Phys. J. Appl. Phys. **24** 215 (2003).  
44  
45 [52] F. Pailloux, D. Imhoff, T. Sikora, A. Barthélémy, J.-L. Maurice, J.-P. Contour, C. Colliex, A.  
46 Fert, Phys. Rev. B **66** 014417 (2002).  
47  
48 [53] V. Garcia, M. Bibes, A. Barthélémy, M. Bowen, E. Jacquet, J.-P. Contour, A. Fert, Phys. Rev.  
49 B **69** 052403 (2004).  
50  
51  
52  
53  
54  
55  
56  
57  
58  
59  
60

- 1  
2 [54] L. Samet, D. Imhoff, J.-L. Maurice, J.-P. Contour, A. Gloter, T. Manoubi, A. Fert, C. Colliex,  
3 Euro. Phys. J. B. **34** 179 (2003).  
4  
5 [55] D. A. Muller, N. Nakagawa, A. Ohtomo, J. L. Grazul, H. Y. Hwang, Nature **430** 657 (2004).  
6  
7 [56] C. Jeanguillaume, C. Colliex, Ultramicroscopy **28** 252 (1989).  
8  
9 [57] M. Abbate, F. M. F. de Groot, J. C. Fuggle, A. Fujimori, G. A. Sawatski, M. Takano, Y.  
10 Takeda, H. Eisaki, S. Uchida, Phys. Rev. B. **46** 4511 (1992).  
11  
12 [58] H. Yamada, Y. Ogawa, Y. Ishii, H. Sato, M. Kawasaki, H. Akoh, Y. Tokura, Science **305** 646  
13 (2004).  
14  
15 [59] M. Abbate, F. M. F. de Groot, J. C. Fuggle, A. Fujimori, Y. Tokura, Y. Fujishima, O. Strebel,  
16 M. Domke, G. Kaindl, J. van Elp, B. T. Thole, G. A. Sawatzki, M. Sacchi, N. Tsuda, Phys. Rev. B.  
17 **44** 5419 (1991).  
18  
19 [60] A. Gloter, A. Douiri, M. Tencé, C. Colliex, Ultramicroscopy **96** 385 (2003).  
20  
21 [61] H. Kurata, C. Colliex, Phys. Rev. B **48** 2102 (1993).  
22  
23  
24  
25  
26  
27  
28  
29  
30  
31  
32  
33  
34  
35  
36  
37  
38  
39  
40  
41  
42  
43  
44  
45  
46  
47  
48  
49  
50  
51  
52  
53  
54  
55  
56  
57  
58  
59  
60

25/06/2010 Maurice et al. : Interfaces in perovskites

Figure captions

Figure 1. The perovskite unit cell  $ABO_3$ , seen with A ions at the corners (a), or B ions at the corners (b). The ion sizes are smaller than in reality but have the right ratios. Oxygen ions that form the octahedra are not drawn in (b) for clarity.

Figure 2. The rhombohedral unit cell of the manganite  $La_{2/3}Sr_{1/3}MnO_3$  (a) still leads to a pseudo-cubic stacking of the oxygen octahedra (b). The crystallographic directions indicated refer to the pseudo cube (where the ‘cubic’ angle is  $90.26^\circ$ ).

Figure 3. Effect of varying the environment of a 3d transition metal at site B on its 3d electron states: the crystal field (CF) of the oxygen octahedron performs a first removal of degeneracy. An additional removal of degeneracy may occur due a lowering of symmetry associated with the Jahn-Teller effect (JT), the epitaxial strain, or to the presence of an oxygen vacancy.

Figure 4. The two types of interfaces obtained when growing a perovskite  $A_fB_fO_3$  on the AO or  $BO_2$  {200} surface of a perovskite  $ABO_3$ . Depending on the valency of the cations, they may have opposite electronic properties (see text).

Figure 5. HRTEM image of the sample analysed in figures 6 to 9.

Figure 6. (a) Variations of electron energy loss fine structure (ELNES) across the LSMO/STO/LSMO stack shown in figure 5, using the spectrum-line technique. The evolutions of the O-1s, Mn-2p and Ti-2p edges across the “bottom” interface (where STO is grown on top of LSMO) is detailed in (b) to (d) respectively, after background subtraction. (The top interface however exhibits very similar features [54].) The spatial distance between spectra is 0.47 nm. An energy deconvolution technique has been used to improve energy resolution [60].

Figure 7. (a) Chemical map of the La to Sr ratio over the LSMO/STO/LSMO junction shown in figure 5. The values were extracted from the La-4d and Sr-4p spectrum images. (b) Profiles averaged parallel to the interfaces of the La/Sr atomic ratio (full line) and of the absolute Mn concentration (full circles). Acquisition time: 10 ms per spectrum. The fact that the two profiles coincide indicates the absence of any significant cation segregation.

25/06/2010 Maurice et al. : Interfaces in perovskites

1  
2  
3  
4  
5 Figure 8. Comparisons of ELNES of O-1s (K-edge) and Ti-2p ( $L_{2,3}$  edge) in the present case  
6 (a, c) and in recordings performed by Muller et al. [55] in  $\text{SrTiO}_{3-\delta}$  samples with varying  
7 oxygen vacancy concentration  $\delta/3$  (b, d). (a) Comparison between the O-K signals in the bulk  
8 of the STO barrier and LSMO films and at the apex of the interfaces: interface signals are  
9 averages of the bulk ones. (b) Comparison of the Ti- $L_{2,3}$  signal from the centre of the barrier  
10 with those at the interfaces, after re-scaling for clarity: there are no significant differences.  
11 Note the sharpness of the peaks in (a) and (c) when compared to the broadening that should  
12 occur in the presence of oxygen vacancies in (b) and (d) (graphs b and d reprinted by kind  
13 permission of David Muller).  
14  
15  
16  
17  
18  
19  
20  
21  
22

23 Figure 9. Evolution of the ELNES of Mn-2p ( $L_{2,3}$ ) edge across the LSMO/STO/LSMO stack  
24 of figure 5, displayed in second derivative mode to exacerbate the fine structure. Spectra  
25 recorded when the centre of the electron probe is 0.9 nm within the barrier (where no Mn is  
26 present) best image interface-specific features. The vertical lines highlight a small amplitude  
27 shift towards lower energies when going from LSMO to the interfaces.  
28  
29  
30  
31  
32  
33  
34  
35  
36  
37  
38  
39  
40  
41  
42  
43  
44  
45  
46  
47  
48  
49  
50  
51  
52  
53  
54  
55  
56  
57  
58  
59  
60

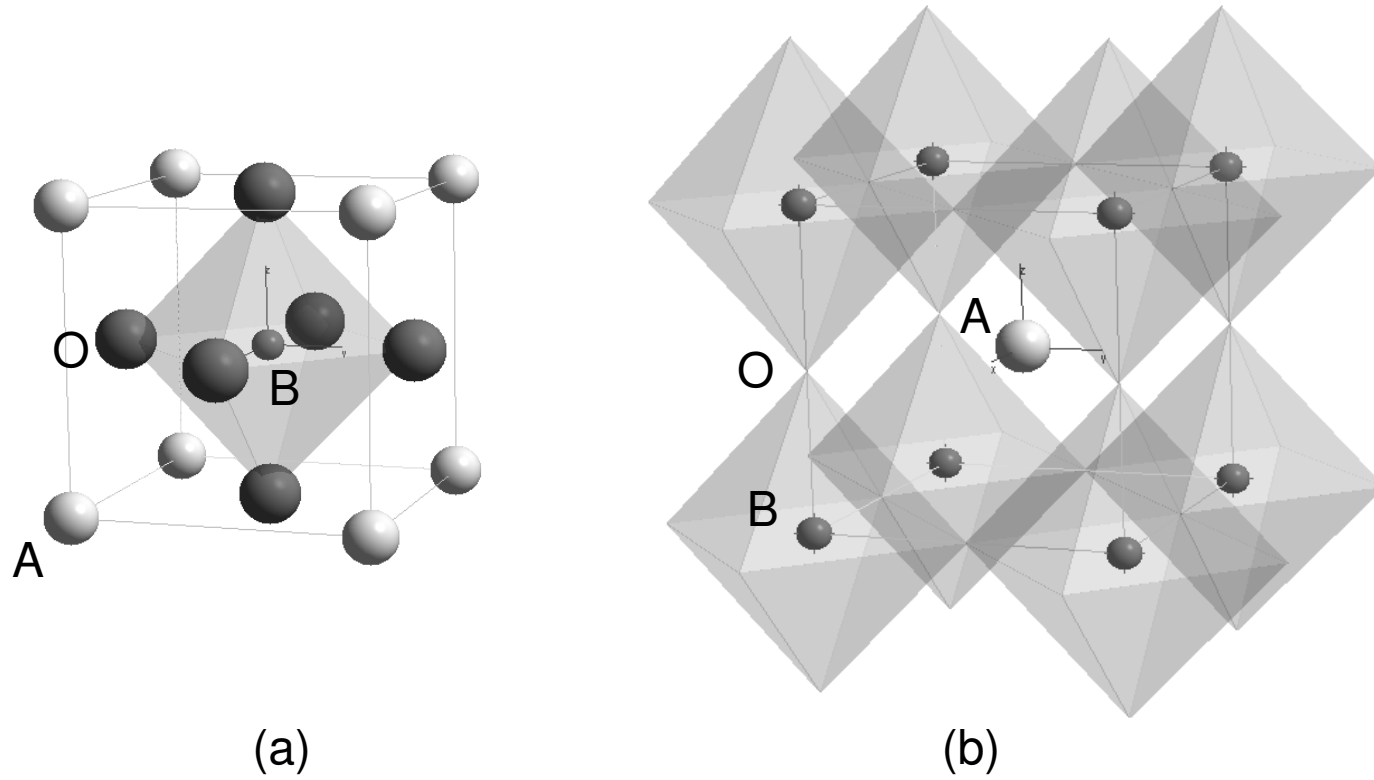


Fig. 1

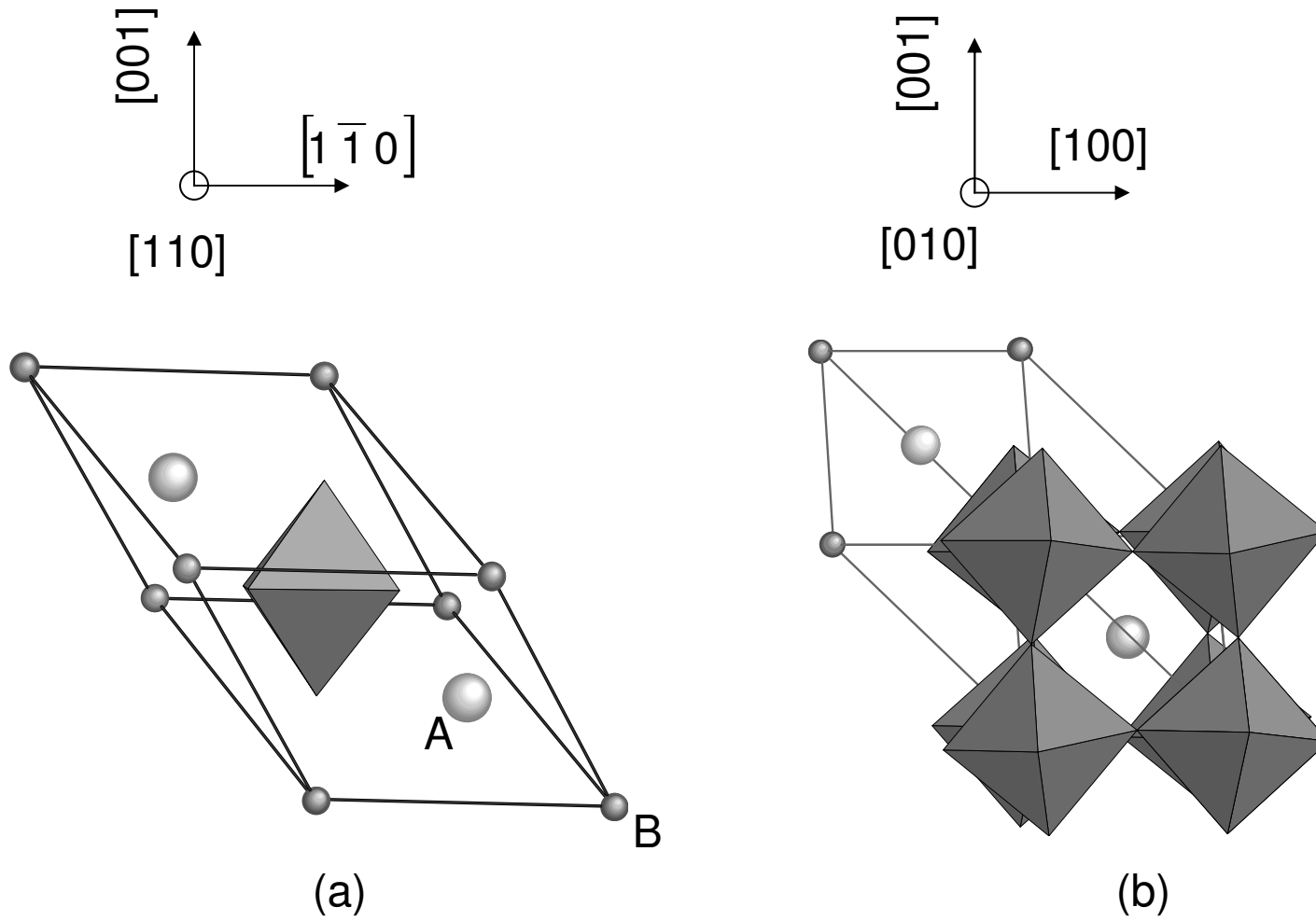


Fig. 2

1  
2  
3  
4  
5  
6  
7  
8  
9  
10  
11  
12  
13  
14  
15  
16  
17  
18  
19  
20  
21  
22  
23  
24  
25  
26  
27  
28  
29  
30  
31  
32  
33  
34  
35  
36  
37  
38  
39  
40  
41  
42  
43  
44  
45  
46  
47  
48  
49

1  
2  
3  
4  
5  
6  
7  
8  
9  
10  
11  
12  
13  
14  
15  
16  
17  
18  
19  
20  
21  
22  
23  
24  
25  
26  
27  
28  
29  
30  
31  
32  
33  
34  
35  
36  
37  
38  
39  
40  
41  
42  
43  
44  
45  
46  
47  
48  
49

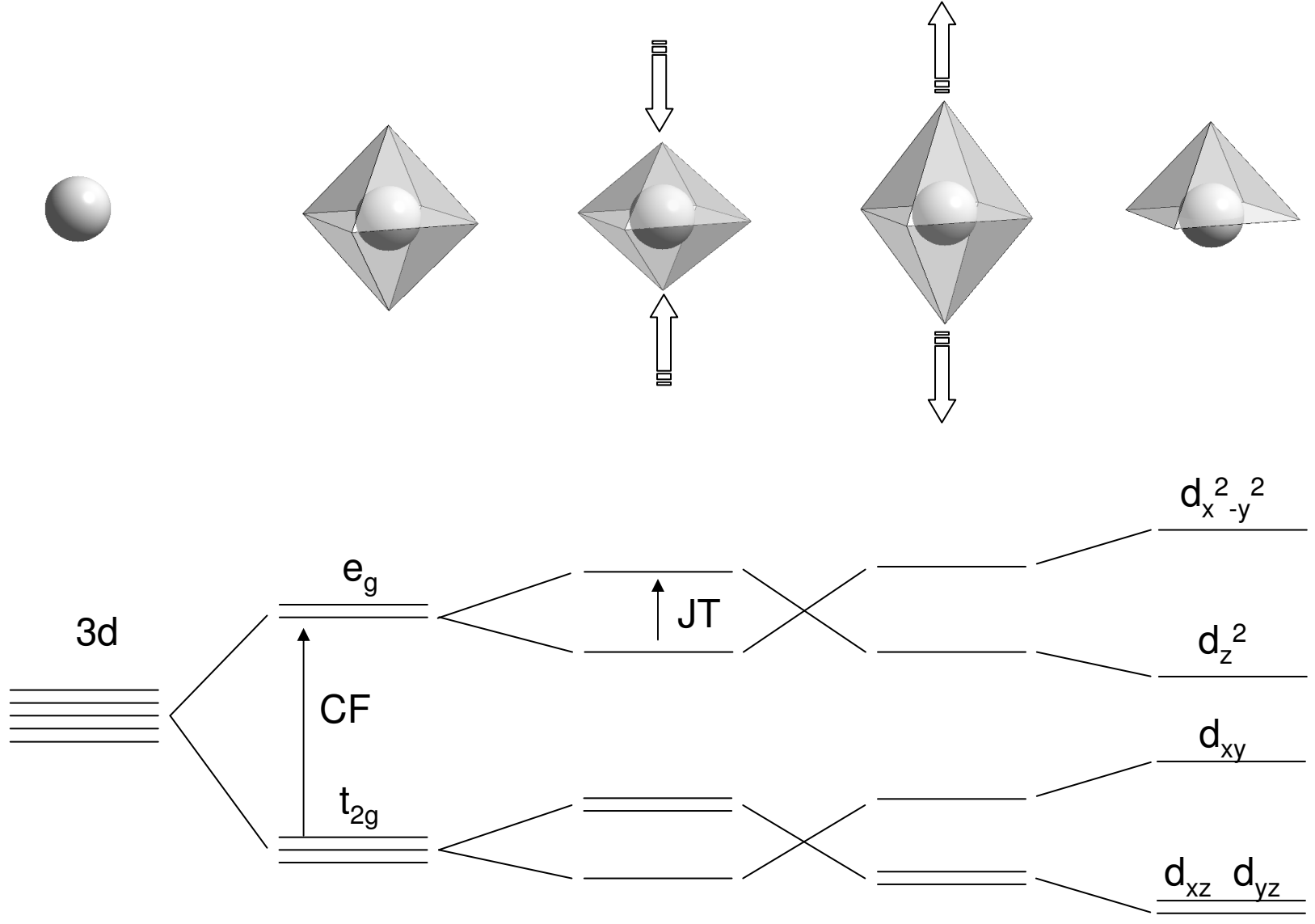


Fig. 3

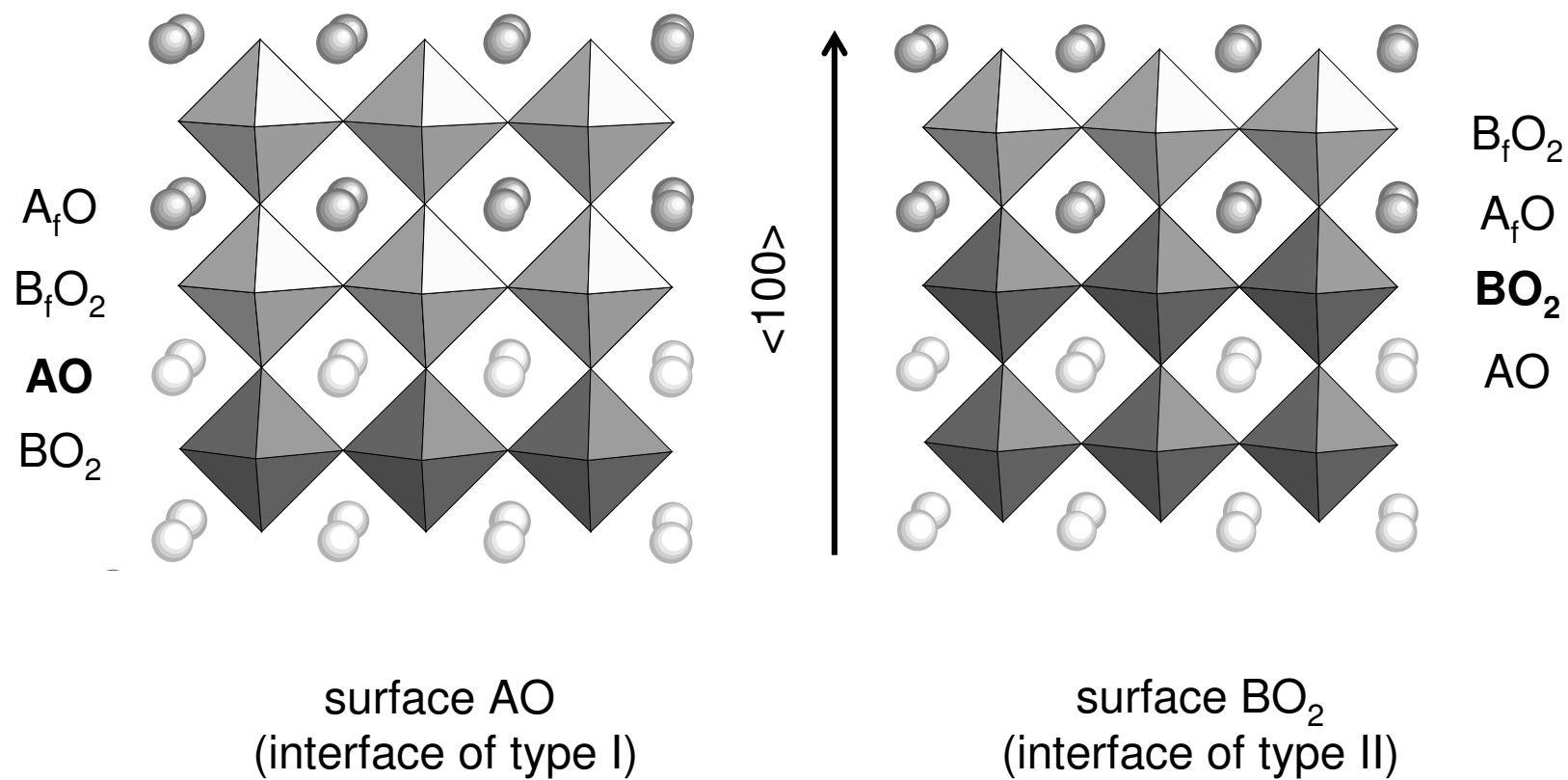


Fig. 4

1  
2  
3  
4  
5  
6  
7  
8  
9  
10  
11  
12  
13  
14  
15  
16  
17  
18  
19  
20  
21  
22  
23  
24  
25  
26  
27  
28  
29  
30  
31  
32  
33  
34  
35  
36  
37  
38  
39  
40  
41  
42  
43  
44  
45  
46  
47  
48  
49

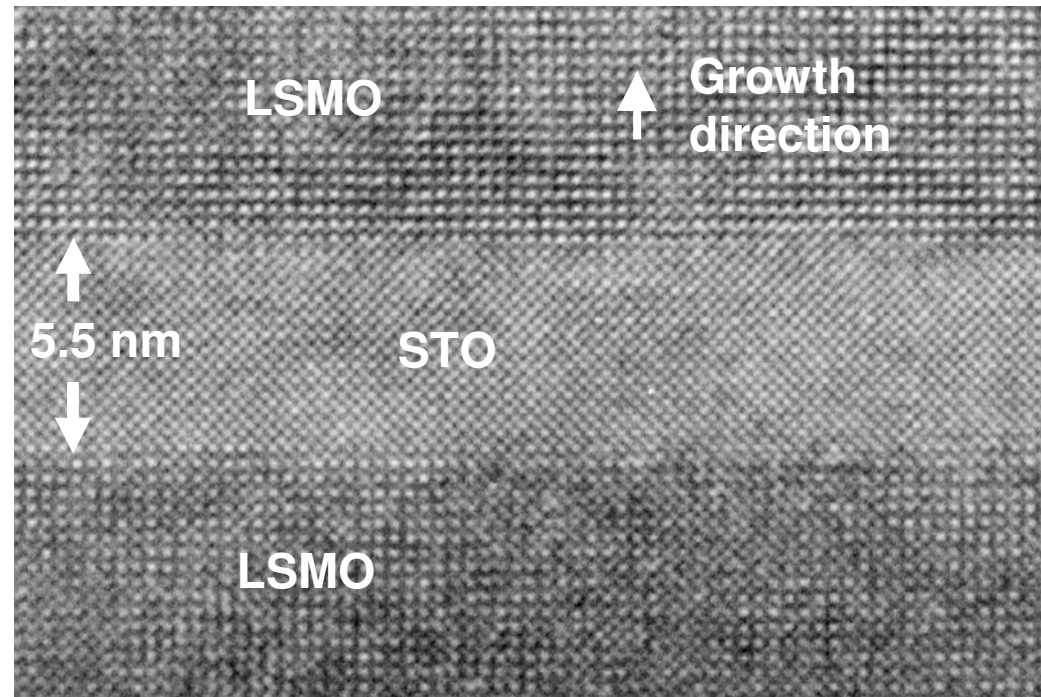


Fig. 5

Maurice et al.: Interfaces in perovskites

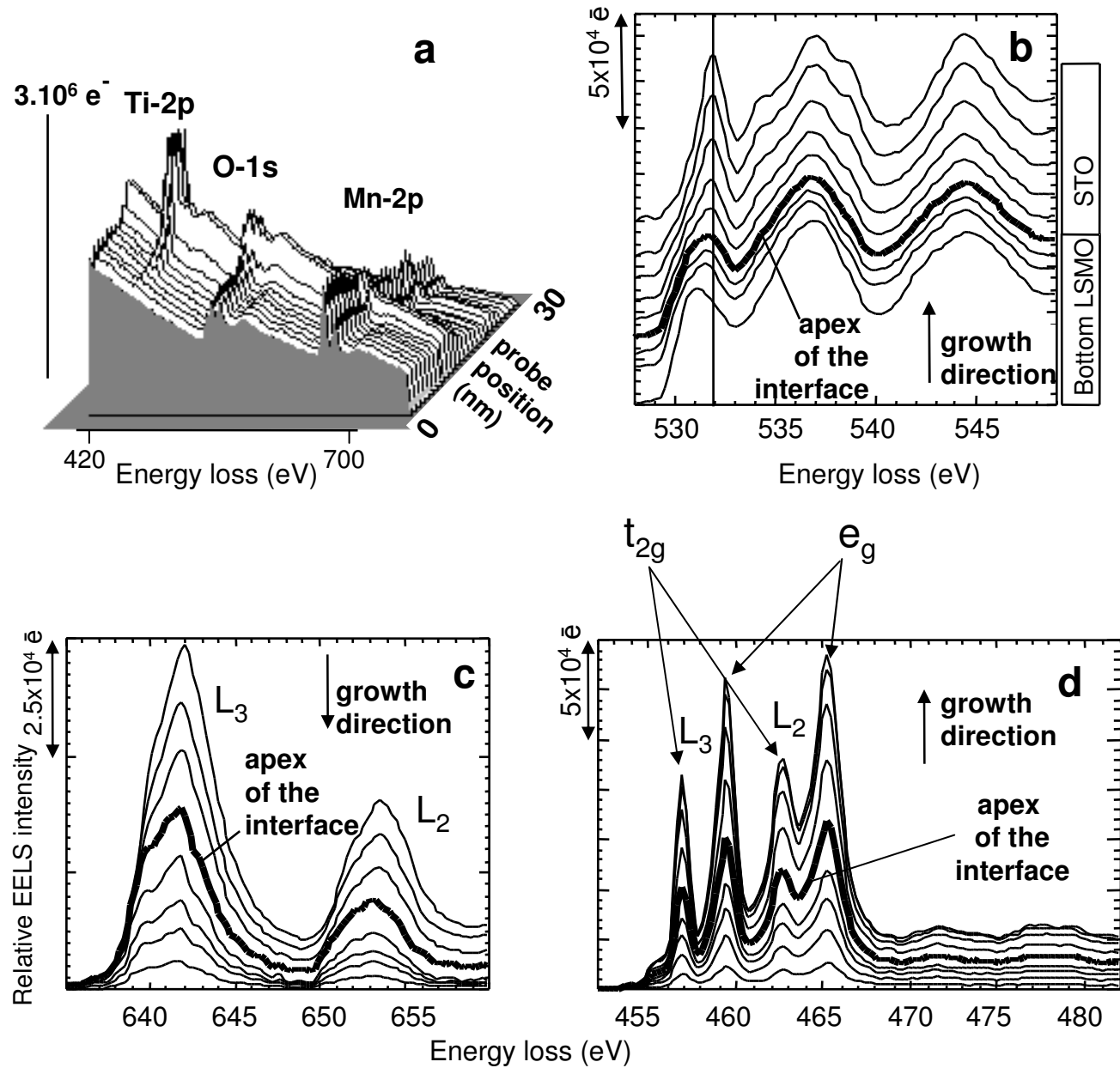


Fig. 6

Maurice et al.: Interfaces in perovskites

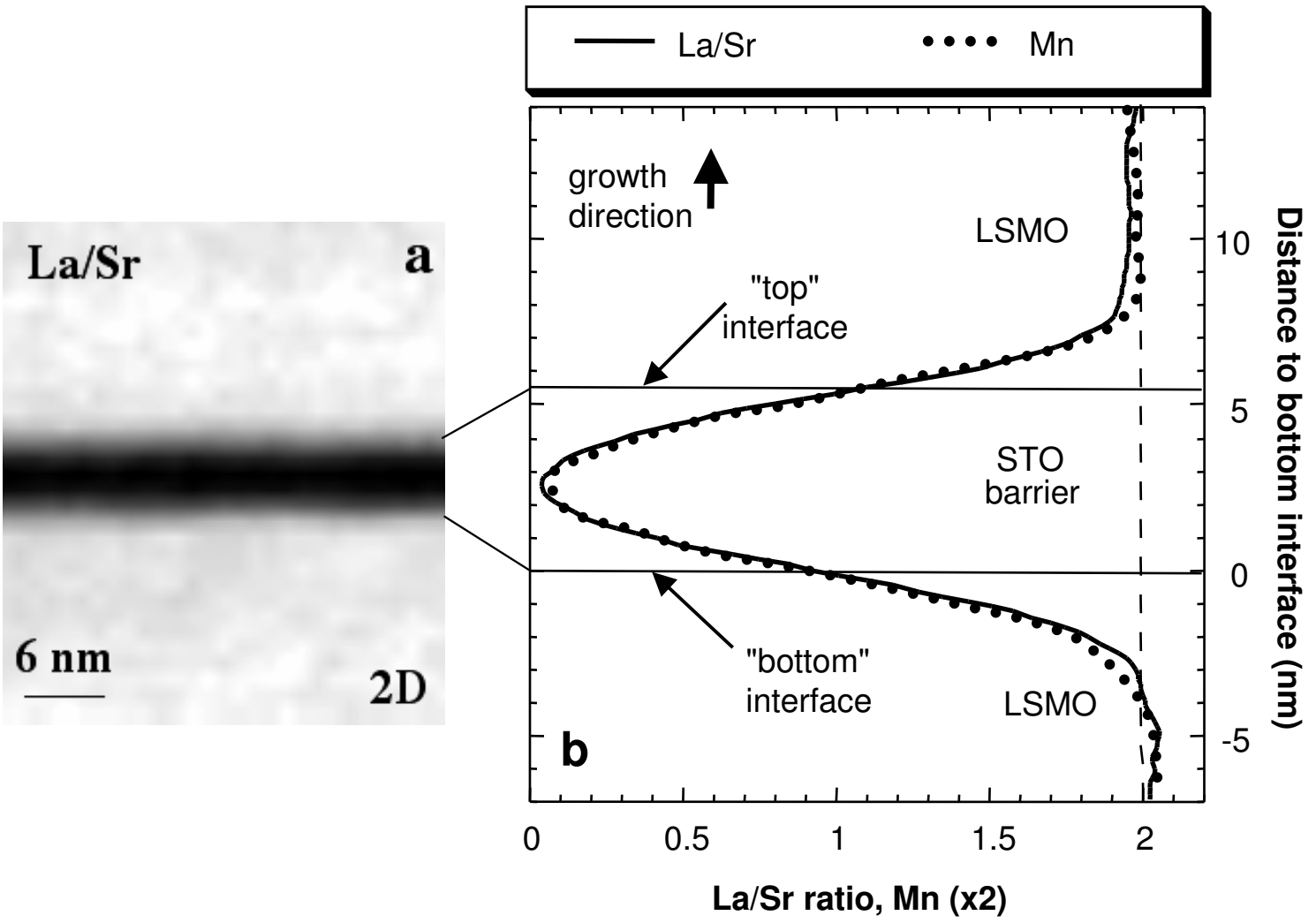


Fig. 7

Maurice et al.: Interfaces in perovskites

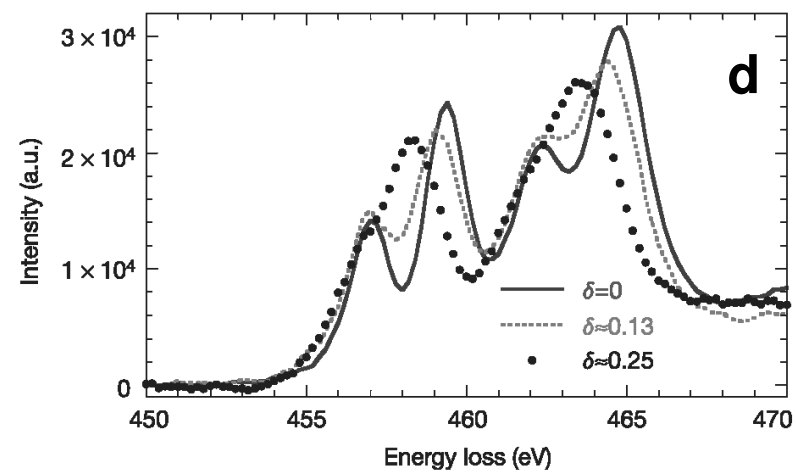
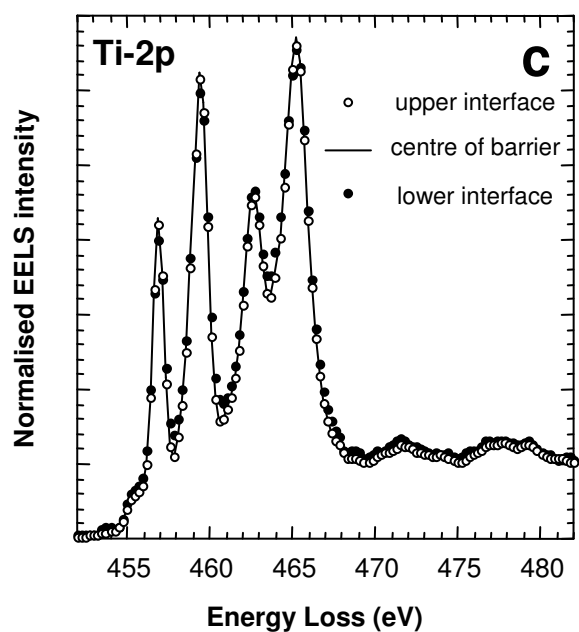
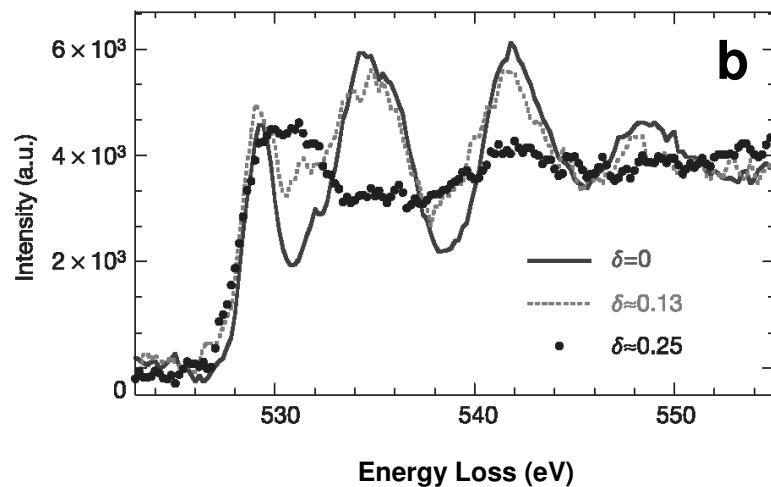
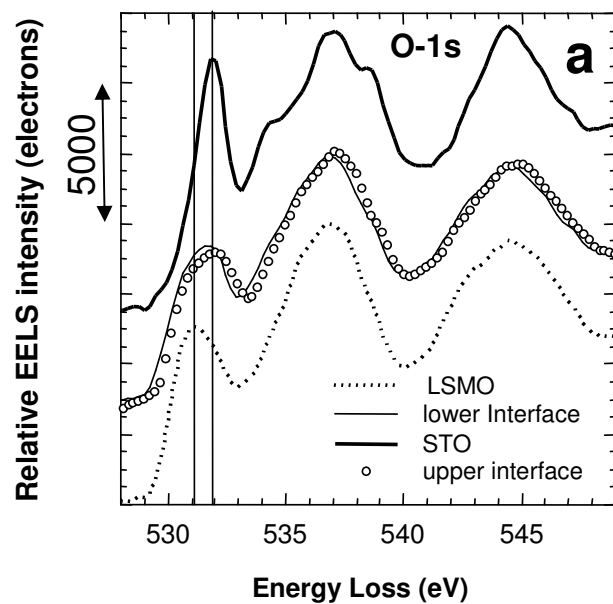


Fig. 8  
Maurice et al.: Interfaces in perovskites

1  
2  
3  
4  
5  
6  
7  
8  
9  
10  
11  
12  
13  
14  
15  
16  
17  
18  
19  
20  
21  
22  
23  
24  
25  
26  
27  
28  
29  
30  
31  
32  
33  
34  
35  
36  
37  
38  
39  
40  
41  
42  
43  
44  
45  
46  
47  
48  
49

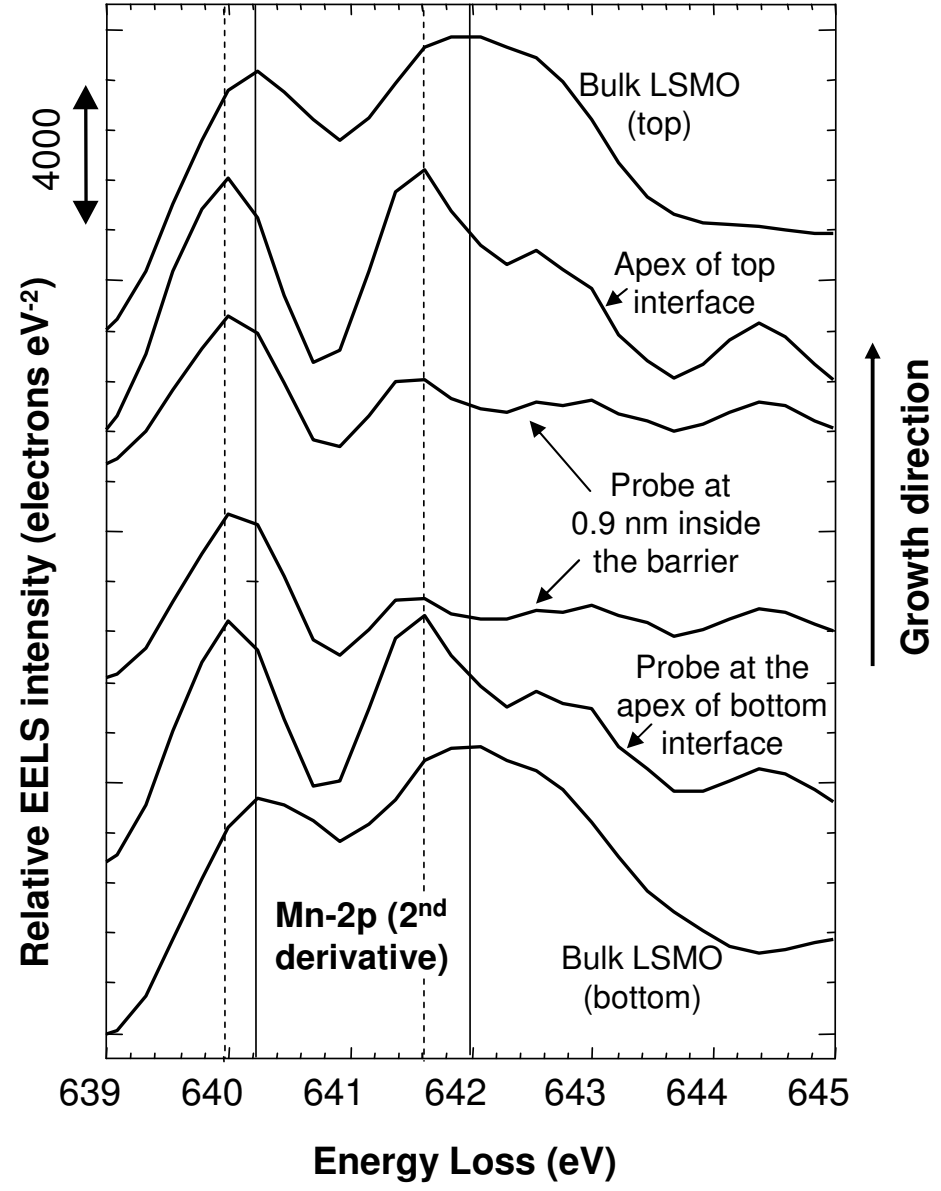


Fig. 9